Control Law Design of a Low-power Wind Energy System Using Active Speed Stall Techniques

Adriana Burlibaşa (Scarlat)*, Iulian Munteanu, Antoneta Bratcu*****

**Dunărea de Jos University of Galati Romania*
(Tel: 0040-336-130-108; e-mail: adriana.scarlat@ugal.ro).
***Grenoble Electrical Engineering Laboratory (G2ELab), France (e-mail: iulian.munteanu@g2elab.grenoble-inp.fr).*
****Grenoble Image, Speech, Signal and Automatic Control (GIPSA-lab), France (e-mail: antoneta.bratcu@gipsa-lab.grenoble-inp.fr).*

Abstract: This paper deals with power control structure design for low power fixed-pitch wind energy conversion systems (WECS) operating in large wind speed variation range. By using variable-speed operation capability, this structure achieves both output power maximization in partial-load regime and power limitation in full-load regime, in this latter case by using active speed stall technique. This control must ensure good dynamic performance in both regimes, as well as smooth transition between them, provided that such transition is accompanied by control phase reversal and also by important plant model changes. This paper proposes a comprehensive design approach of the respective power controllers and an original switching mechanism ensuring smooth transition. The experimental results performed on a dedicated test rig show good dynamic performance, being obtained regardless of the wind speed and the operating regime.

Keywords: windmills, power control, non-minimum phase systems, root-locus, variable structure control

1. INTRODUCTION

The wind energy conversion systems (WECS) are electrical power generation structures with an uneasy task due to the combination between the stochastic evolutions of the wind speed and the intrinsic nonlinearities of the aerodynamic characteristics. The WECS control must ensure power limitation in full-load regime, *i.e.* in Region 3 of the power-wind speed characteristic (Şerban *et al.* (2012)). Usually, this is performed by bringing the wind turbine operation mode in feathering regime through pitch control, (Burton *et al.* (2001), Munteanu *et al.* (2008)). In partial-load regime, *i.e.* in Region 2 of the mentioned power characteristic, wind energy conversion optimization is performed by keeping the operating point on the optimal regime characteristic (ORC) (Munteanu *et al.* (2008), Bianchi *et al.* (2006)). For this purpose, a control loop that maintains the electromagnetic torque or the electromechanical power close to the optimal values – computed based on the measured rotational speed – is usually employed (Burton, T. *et al.* (2001), Munteanu *et al.* (2008)).

Nowadays, the low-power grid WECS begin to play an important role in the decentralized production of electrical energy. In these systems, standard limiting of the captured power in full-load regime through pitch angle control is expensive. For small wind turbines, power limitation is made usually by passive stall, using an appropriate aerodynamic blade profile that reduces the aerodynamic tangential force while operating beyond the rated wind speed (Burton *et al.* (2001), Bianchi *et al.* (2006)). However, the performance of this solution is reduced. The recently developed variable-speed capability of WECS has enabled the output power regulation – also called active speed stall control – in high winds by inducing aerodynamic stall effect (Munteanu *et al.* (2008), Hoffman (2002), Vihriälä (2002), Bang *et al.* (2007), Polinder *et al.* (2007)).

In this paper a low-power off-grid WECS is considered, where both power limitation and power maximization are implemented by acting on the rotational speed through the variable-speed control infrastructure. The proposed control structure is implemented by means of output power control loop that ensures WECS operation over the entire wind speed variation range.

A systematic design procedure of the power controller for both operating regimes is here proposed. This problem is not trivial, because switching between the mentioned regions involves a radical change in properties of the controlled process, this latter becoming a non-minimum phase system in Region 3. The proposed control solutions are validated experimentally on a rig test.

The paper is organized as follows. Section 2 presents the WECS configuration and details the modelling and design of the low-level control loops. Section 3 deals with the power controller design in each of the two main operating regimes. Section 4 allows the analysis of the experimental results concerning the system closed-loop dynamical behaviour. Finally, Section 5 is dedicated to conclusions.

2. MODELLING AND DESIGN OF THE LOW-LEVEL CONTRL LOOPS

2.1 WECS structure

The studied WECS is composed of a fixed-pitch wind turbine directly coupled to a permanent-magnet synchronous generator (PMSG) which can be driven at variable speed via a diode rectifier and a DC-DC buck power stage. It supplies a DC bus to which an isolated AC load is connected by means of stand-alone inverter (Fig. 1a). A battery accumulator is also connected to the DC-bus.

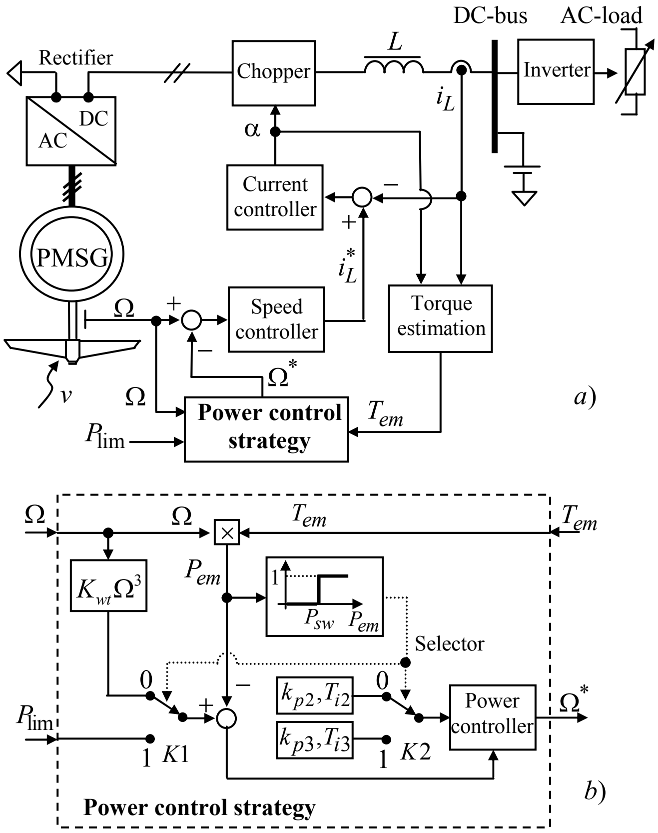

Fig. 1. Three-loop cascaded control structure in which the power control is achieved by means of a single PI controller with switched parameters

The cascaded control structure uses on the outermost layer the power loop; its controller feeds the inner rotational speed loop with the speed reference. A standard speed control for AC machines is used, which is based on the innermost terminal current control loop. In the present case, this current is controlled by means of the buck converter (see Fig. 1a).

The power control structure is depicted in Fig. 1b and allows WECS operation within the entire wind speed range, as described below.

When the system operates in partial-load regime and the wind speed increases, the power loop controller used to ensure ORC operation imposes the rotational speed increasing. In full-load regime, reached when the wind speed becomes greater then the rated, the power captured limitation, performed through active stall speed control strategy, requires rotational speed decrease. Therefore the switching between power optimization and power limitation regimes and vice versa is performed by reversing the phase command of power controller. To avoid unstable system behaviour and also to ensure smooth transition of state variables at the commutation between these operating regimes, it is considered an intermediate region where the rotational speed is kept constant to a reference imposed by the saturated power controller command. Therefore partial-load regime is composed of Region 2a, which covers system operation on the ORC, see region A-B from Fig. 2, and Region 2b, corresponding to the region B-C from Fig. 2, where rotational speed is limited to a constant value. Also from Fig. 2 can be seen the Region 3 described by C-D region, which covers power limitation system operation. The commutation between Region 2b and Region 3 through a power controller with switching parameters is achieved.

Aerodynamic wind turbine model is given by the wind torque, T_w :

$$T_w(v,\Omega) = 0.5\pi\rho R^3 v^2 C_T(\lambda), \tag{1}$$

where $C_T(\lambda)$ is the torque coefficient, λ is the tip speed ratio ($\lambda = R \cdot \Omega / v$, with Ω the rotational speed, v the wind speed and R the blade length). In this paper, the torque coefficient is a polynomial function of λ (Vlad *et al.* (2009), Munteanu *et al.* (2008)):

$$C_T(\lambda) = a_6 \cdot \lambda^6 + a_5 \cdot \lambda^5 + a_4 \cdot \lambda^4 + a_3 \cdot \lambda^3 + a_2 \cdot \lambda^2 + a_1 \cdot \lambda + a_0, \tag{2}$$

where the numerical values of $a_i, i = \overline{0,6}$ are given in Appendix. The aerodynamic torque characteristics of the considered wind turbine are given in Fig. 2 (with thin continuous line) and also the ORC (with doted line).

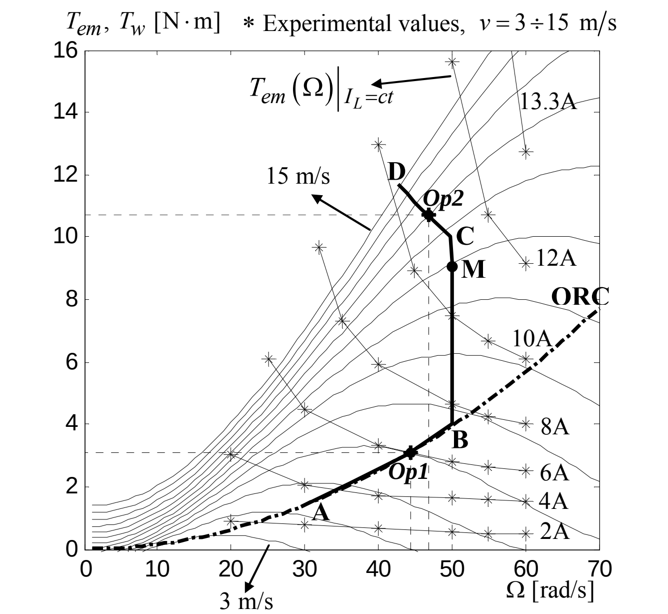

Fig. 2. Steady-state WECS torque characteristics

The proposed control structure consists of the current control loop (innermost), the rotational speed control loop, which ensure the WECS stable operation, and the power control loop. The rotational speed reference is given by the Power Control Strategy (PCS). This bloc belongs to the outer power loop, characterised by switchable parameters and power reference depending on the operating regime.

The current established in the DC-DC buck inductor, i_L, is controlled by a PI controller with antiwindup. The current controller parameters are given in Appendix. The presence of the current loop within the controlled rectifier shapes the mechanical characteristics of the PMSG.

The PMSG electromagnetic torque, T_{em}, is proportional with the chopper current, i_L and the converter duty ratio α: $T_{em} = k_T(\alpha)\cdot\alpha\cdot i_L$, where k_T is a parameter defined experimentally in relation with the buck converter duty ratio, α. The experimentally determined $k_T(\alpha)$ is shown in Fig. 3.

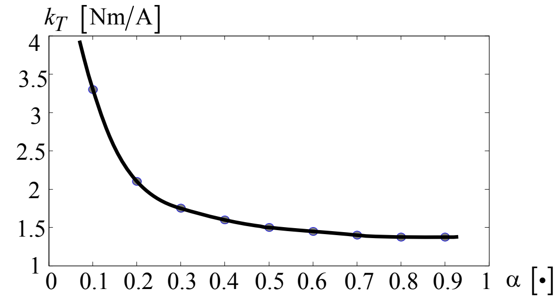

Fig. 3. Coefficient expressing the current-torque dependence as function of the converter duty ratio.

The electromagnetic torque characteristics, $T_{em}(\Omega, i_L)$, of the considered WECS, are experimentally obtained and represented in Fig. 2 (the experimental points are marked with stars).

The operating point trajectory A-B-C-D, given in Fig. 2, is obtained for a sufficiently slow positive ramp variation of the wind speed. This is useful to detail the outer power loop operation and the rotational speed reference generation by the PCS block (see Fig. 1b). Region A-B corresponds to Region 2a where wind system operation is on the ORC. In this region, the power reference is $P_{em}^* = K_{wt}\cdot\Omega^3$, where $K_{wt} = 0.5\rho\pi\cdot\left(C_p\left(\lambda_{opt}\right)/\lambda_{opt}^3\right)\cdot R^5$, with $C_p\left(\lambda_{opt}\right)$ being the maximum power coefficient value, obtained for the value of the optimal tip speed ratio, λ_{opt} (Vlad *et al.* (2009)). In this case the antiwindup power controller successively increases the reference Ω^*, generating a displacement to right of the operating point. When the power controller output is limited and the imposed reference is $\Omega^* = \Omega_{lim}$, the system operates in region B-C corresponding to Region 2b. A positive increase of wind speed generates an upward displacement of the operating point. When wind system operation is performed in region C-D, corresponding to Region 3, the variation sense of the rotational speed reference Ω^* must be reversed. To avoid instability behaviour and to ensure a smooth commutation between operating regimes, a point below C must be considered as a commutation point, noted with M. It corresponds to the power switch value P_{sw} (see Fig. 2). Before commutation, in both regions A-B and B-M, K1 and K2 switchers of PCS are in the position 0 and therefore the power controller parameters are k_{p2} and T_{i2}, and the power reference is $P_{em}^* = K_{wt}\cdot\Omega^3$. When the electromagnetic power becomes equal with P_{sw}, K1 and K2 are switched in position 1. Practically a simultaneous commutation to k_{p3} and T_{i3} parameters and to $P_{em}^* = P_{lim}$ power reference is provided. It should be noted that the parameter k_{p3} has opposite sign in relation to k_{p2}. The parameters pair (k_{p3}, T_{i3}) is specific to M-C and C-D regions. Before switching, the power loop error is negative: $\varepsilon_P = K\Omega^3 - P_{em} = K\Omega_{\lim}^3 - P_{em} < 0$. At the commutation, the error becomes positive $\varepsilon_P = P_{\lim} - P_{em} = P_{\lim}^* - P_{sw} > 0$. Trough a simultaneous reverse of power error sign and of the output power controller phase (given by the sign reverse of the power controller proportional gain), the sign of the controller command is kept unchanged. In addition, because the power controller output is kept to the limitation value, the commutation has no disturbing effects to the other control loops subordinated to the power loop. Therefore the instability is avoided and a smooth commutation between the operating regions is provided.

2.2 Rotational speed controller design

As shown in Fig. 1, the chopper current reference is provided as the output of the rotational speed controller in a cascade control structure. The i_L current dynamics are sufficiently fast in order to be neglected in the speed control loop design. The motion equation of the wind turbine-PMSG coupling is:

$$J\frac{\mathrm{d}\Omega}{\mathrm{d}t} = T_w(\Omega, v) - T_{em}(\Omega, i_L), \tag{3}$$

where J is the inertia moment. Both steady-state family characteristics $T_w(\Omega, v)$ and $T_{em}(\Omega, i_L)$ are essential for estimating the linearized system parameters.

Let $\overline{\bullet}$ denote the value of a variable in a given operating point. For small variations around a typical operating point, the linearized model of the wind turbine is:

$$\Delta\Omega(s) = \frac{k_w K}{Ts+1}\cdot\Delta v(s) - \frac{k_{em}K}{Ts+1}\cdot\Delta i_L(s), \tag{4}$$

where

$$K = 1\Big/\left(\overline{\partial T_{em}/\partial\Omega} - \overline{\partial T_w/\partial\Omega}\right); \quad T = J\cdot K \tag{5}$$

are the gain and the system time constant respectively and

$$k_w = \overline{\partial T_w/\partial v},\ k_{em} = \overline{\partial T_{em}/\partial i_L} \tag{6}$$

It is used $\overline{\partial T_{em}/\partial\Omega}$ for the electromagnetic torque characteristic slope, $\overline{\partial T_w/\partial \Omega}$ for the wind turbine torque characteristic, $\overline{\partial T_w/\partial v}$ for the wind turbine torque variation in relation to wind speed variation, and $\overline{\partial T_{em}/\partial i_L}$ for the electromagnetic torque variation in relation to load current variation.

By examining the desired operating locus in Fig. 2, one can remark that the torque curve slopes significantly change from partial-load to full-load regime, while they do not change very much inside of each region. The time constant T can be positive or negative, depending on where the operating point should be established: either on the ascending part of the wind torque curve or on its descending part. Hence the plant having the current i_L as input and the rotational speed Ω as output varies strongly, becoming unstable in full load (Scarlat *et al.* (2010)).

The control design procedure is based upon using the above linearized model– see Fig. 4 – and aims at finding a single PI controller which performs robustly in both partial- and full-load regimes. Let k_p and T_i be the proportional gain and the integral time constant of a PI rotational speed controller.

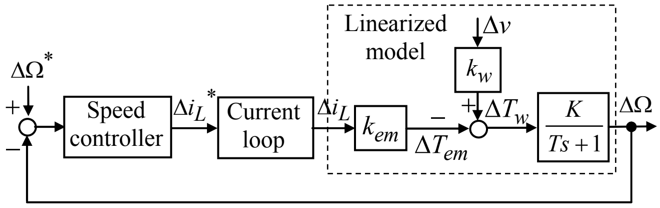

Fig. 4. Linearized model of the rotational speed control loop

These parameters can be computed through the classical pole-placement method (Åström *et al.* (1995)). The system's closed loop transfer function is:

$$H_{0\Omega}(s) = \frac{(T_i s+1)k_p k_{em} K}{-T.T_i s^2 + T_i(k_p k_{em} K - 1)s + k_p k_{em} K} = \frac{(T_i s+1)}{T_0^2 s^2 + 2\varsigma T_i s + 1} \tag{7}$$

Imposing the pairs of poles defined by the time constant T_0 and the damping factor ς_0, one may deduce:

$$k_p = \left(1 - 2\varsigma_0 T/T_0\right)/(k_{em}K); \quad T_i = -T_0^2/T + 2\varsigma_0 T_0 \tag{8}$$

Relations (8) show obviously that the controller parameters depend on the operating point; moreover, in our case, they will also depend strongly on the operating regime. This means that a certain desired dynamic performance will be obtained with different sets of controller parameters, depending on the operating regime. Next, a qualitative procedure is proposed in order to choose the most suitable set of controller parameters. Thus, two operating points are chosen, each of which is typical for Region 2a and Region 3 respectively. Two pairs $\left(k_p, T_i\right)$ are computed accordingly by using (8). Then the performance of each such controller is assessed by numerical simulation in the other region. Finally, the parameter set ensuring the minimal performance degradation is chosen. Fig. 2 identifies two typical operating points placed in Region 2a and Region 3 respectively; these are:

$$\begin{cases} op_1 = \left(\Omega, T_{em}, v\right) = \left(44.4 \text{ rad/s},\ 3.1 \text{ Nm},\ 6 \text{ m/s}\right) \\ op_2 = \left(\Omega, T_{em}, v\right) = \left(46.8 \text{ rad/s},\ 10.7 \text{ Nm},\ 12 \text{ m/s}\right) \\ M = \left(\Omega, T_{em}, v\right) = \left(50 \text{ rad/s},\ 9 \text{ Nm},\ 9.9 \text{ m/s}\right) \end{cases} \tag{9}$$

In (9) it is also mentioned the point M where the commutation between the main operating regimes is performed. For each of these two operating points a transfer function is derived. To deduce the transfer functions' parameters, the slopes $\overline{\partial T_w/\partial \Omega}$, $\overline{\partial T_{em}/\partial \Omega}$, $\overline{\partial T_w/\partial v}$ and $\overline{\partial T_{em}/\partial i_L}$ corresponding to the chosen operating points are estimated based upon curves in Fig. 2; Table 1 presents the results.

Based on (8), Table 1 and the chosen values for ς_0 and T_0, the rotational speed controller parameters can be computed. For example, by imposing $\varsigma_0 = 0.6$ and $T_0 = 0.3$ s, one obtains: for Region 2a: $k_p = -0.78$ and $T_i = 0.33$ s; for Region 3: $k_p = -0.47$ and $T_i = 0.82$ s.

Table 1. Parameter estimation for two operating points

Slopes	Operating point in Region 2 – op_1		Operating point in Region 3 – op_2	
$\overline{\partial T_w/\partial \Omega}$	–0.125	$K = 13.52$	0.2350	$K = -0.9761$
$\overline{\partial T_{em}/\partial \Omega}$	–0.051		–0.7895	
$\overline{\partial T_w/\partial v} = k_e$	1.615	$T = 2.7$	0.884	$T = -0.1952$
$\overline{\partial T_{em}/\partial i_L} = k_{em}$	0.925		3.898	

These two obtained rotational speed control loops, specific to each operating regime, are simulated in both regimes. Step responses are shown in Fig. 5. To mitigate overshoots it is usual to pass the reference through a first-order pre-filter, with the time constant T_i in this case. One can note that the parameter set ensuring the minimal performance degradation in the other operating regime is the one associated to Region 2a. It is this set of parameters that is used for implementing the rotational speed controller.

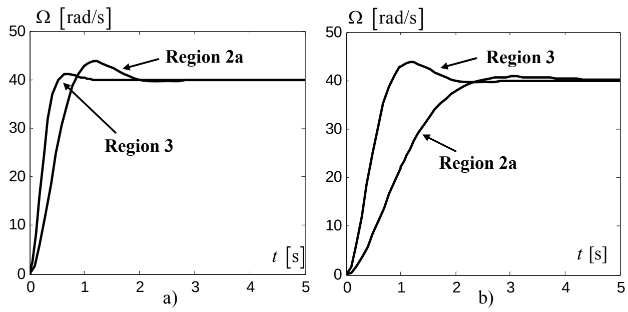

Fig. 5. Closed-loop rotational speed behaviour corresponding to controller for the operating point being placed respectively in: a) Region 2a; b) Region 3.

3. MODELLING AND DESIGN OF THE POWER CONTROL LEVEL

3.1 Modelling

The outermost (power) control loop establishes the turbine operating point position. As Fig. 1 and Fig. 6.a show, it is about an autonomous closed-loop system driven only by its disturbance, the wind speed. The control input is the rotational speed setpoint and the output is the electromagnetic power. The feedback has different structures for the two main operating regimes as Fig. 6a shows. The same PI controller is used in both regions, whose set of parameters switches between (k_{p2}, T_{i2}) in Region 2 and (k_{p3}, T_{i3}) in Region 3. Derivation of plant models for both of regions is thus needed.

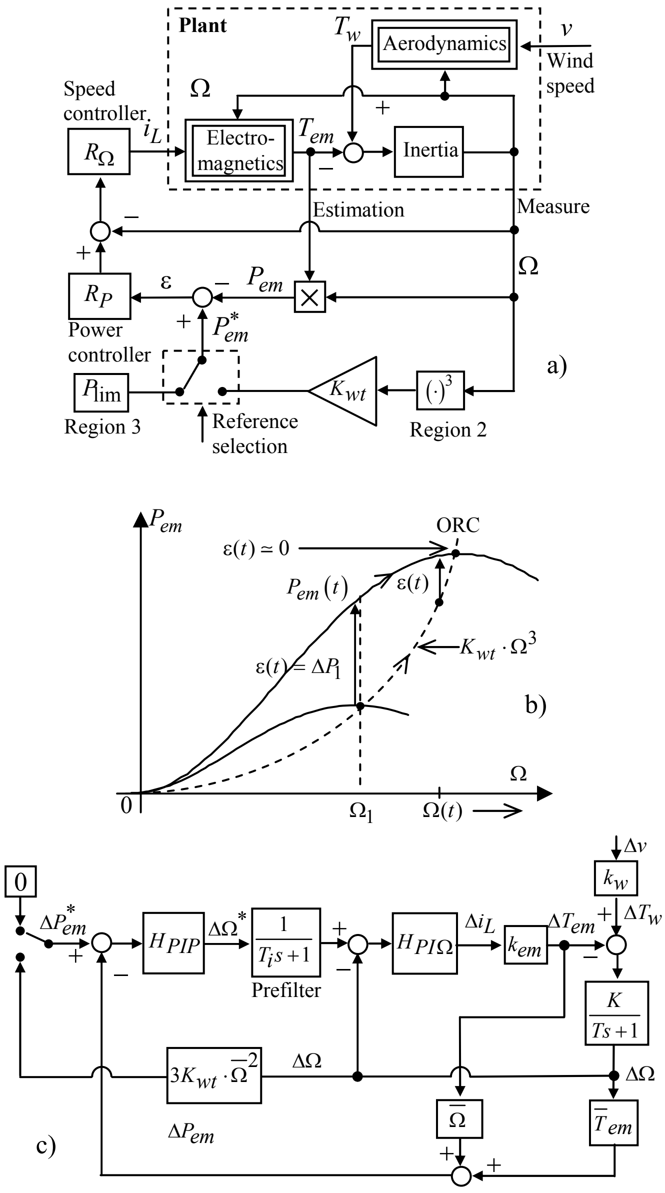

Fig. 6. The power control loop: a) at the transition between partial load and full load b) zeroing of the power error in partial-load operation when a step disturbance in the wind speed occurs; c) linearized closed-loop block diagram.

First, let us consider the system analysis in Region 2 (partial load). The control error in this case is: $\varepsilon = P^*_{em} - P_{em}$, where the power reference is $P^*_{em} = K_{wt}\cdot\Omega^3$. In closed loop, both variables P_{em} and P^*_{em} evolve towards a certain equilibrium point as the rotational speed reference varies. If considering a wind speed step variation occurring at the rotational speed Ω_1, the electromagnetic power is affected immediately; in this way, the operating point jumps towards the new power characteristic and the error becomes $\varepsilon = \Delta P_1$ (see Fig. 6b). If the power controller demands a speed increase, the error ε evolves toward zero as it can be seen in Fig. 6b. A controller with proportional-integral action should be able to zeroing the power error; let $H_{PIP}(s)$ be its transfer function.

In order to analytically compute the controller parameters, one proceeds towards the system linearization around a typical operating point. The electromagnetic power expression is $P_{em} = \Omega\cdot T_{em}$, which leads to the electromagnetic power variation around the operating point being expressed as:

$$\Delta P_{em} = \overline{T_{em}}\cdot\Delta\Omega + \bar{\Omega}\cdot\Delta T_{em} \tag{10}$$

In a similar way:

$$\Delta P_{em}{}^* = 3K_{wt}\bar{\Omega}^2\cdot\Delta\Omega \tag{11}$$

By combining (10) and (11) the power error results:

$$\Delta\varepsilon = \Delta P^*_{em} - \Delta P_{em} = \underbrace{\left(3\bar{\Omega}^2 K_{wt} - \overline{T_{em}}\right)}_{m}\cdot\Delta\Omega - \bar{\Omega}\cdot\Delta T_{em} \tag{12}$$

where variable

$$m = 3\bar{\Omega}^2 K_{wt} - \overline{T_{em}} \tag{13}$$

has torque dimension. From the rotational speed control loop diagram in Fig. 4 it results that:

$$\Delta\Omega = \frac{K}{Ts+1}\cdot\left(-\Delta T_{em} + \Delta v\cdot k_w\right), \tag{14}$$

where K and T are defined in (5) and k_w is defined in (6). Extracting ΔT_{em} from (14) and replacing it into (12) gives:

$$\Delta\varepsilon = \left[m + \frac{\bar{\Omega}}{K}(Ts+1)\right]\cdot\Delta\Omega - \bar{\Omega}\cdot k_w\cdot\Delta v\,, \tag{15}$$

where one takes account that $\Delta\Omega$ is obtained by passing the reference $\Delta\Omega^*$ through the transfer function (7) and a pre-filter. Hence:

$$\Delta\varepsilon = \left[m + \frac{\bar{\Omega}}{K}(Ts+1)\right]\cdot\frac{1}{T_0^2 s^2 + 2\varsigma_0 T_0 s + 1}\cdot\Delta\Omega^* - \bar{\Omega}\cdot k_w\cdot\Delta v \tag{16}$$

This relation shows that the power error variation evolves as function of the plant's two inputs in the considered operating point – *i.e.*, the rotational speed reference variation and the wind speed variation – by means of gains changing with the current operating point. T_0 and ς_0 are the rotational speed loop parameters computed at the same operating point. Using (5) and (16), the transfer function from the rotational speed reference to the power error variation is given by:

$$H_{\varepsilon\Omega}(s) = \frac{\Delta\varepsilon}{\Delta\Omega^*} = \left(m + \overline{\Omega}/K\right) \cdot \frac{\dfrac{\overline{\Omega} \cdot J}{m + \overline{\Omega}/K} s + 1}{T_0^2 s^2 + 2\varsigma_0 T_0 s + 1} \tag{17}$$

The denominator of this transfer function is the same as the one of the rotational speed closed loop. Therefore the plant properties change with the operating point. In operating Region 2 the gain expression $m + \overline{\Omega}/K = 3\overline{\Omega}^2 K_{wt} - \overline{T_{em}} + \overline{\Omega}/K$ results positive as in general the first term is about ten times larger than the second one for the low-power turbines (kW-order) operating at low rotational speed (tens of rad/s). The third term is positive, being the smallest in the above expression (about few N·m). From (17) one can deduce that the previously analyzed gain determines the nature of the transfer function zero. In Region 2 the $H_{\varepsilon\Omega}$ transfer function zero is stable and variant with the operating point, corresponding to a rather compliant dynamic behaviour.

Note also that (17) represents a general equation which characterizes the system operation in both Regions 2 and 3. As in Region 3 the power setpoint is constant ($\Delta P_{em}^* \equiv 0$), the feedback network changes and (17) holds with $m = -\overline{T_{em}}$ (see Fig. 6c). In aerodynamic stall the expression $m + \overline{\Omega}/K = -\overline{T_{em}} + \overline{\Omega}/K$ is strictly negative as the second term is negative (see Table 1).

Table 2. Parameters in (17) depending on the operating region

Region 2a	Region 3
Parameters	
$K = 13.52 > 0$; $T = 2.7 > 0$	$K = -0.98 < 0$; $T = -0.2 < 0$
$k_p = -0.78 < 0$; $T_i = 0.33 > 0$	$k_p = -0.78 < 0$ $T_i = 0.33 > 0$;
$m = 3\overline{\Omega}^2 K_{wt} - \overline{T_{em}} = 6.23 > 0$	$m = -\overline{T_{em}} = -10.7<0$
$\left(m + \overline{\Omega}/K\right) = 9.51 > 0$	$\left(m + \overline{\Omega}/K\right) = -58.7<0$
$\dfrac{\overline{\Omega} \cdot J}{m + \overline{\Omega}/K} = 0.935 > 0$	$\dfrac{\overline{\Omega} \cdot J}{m + \overline{\Omega}/K} = -0.16 < 0$
$T_0^2 = -\dfrac{T \cdot T_i}{k_p k_{em} K} = 0.09 > 0$	$T_0^2 = -\dfrac{T \cdot T_i}{k_p k_{em} K} = 0.145 > 0$
$2\varsigma_0 T_0 = T_i\left(1 - \dfrac{1}{k_p k_{em} K}\right) = 0.36 > 0$	$2\varsigma_0 T_0 = T_i\left(1 - \dfrac{1}{k_p k_{em} K}\right) = 0.22 > 0$
Poles and zero	
$p_{1,2} = -2 \pm 2.66i$; $z = -1.07$	$p_{1,2} = -5.075 \pm 4.58i$; $z = 6.265$

This means that the $H_{\varepsilon\Omega}(s)$ gain becomes negative in Region 3. So, in order to maintain a stable operation, the power controller must also change its sign when switching from Region 2 to Region 3. Also, the analysis of $m + \overline{\Omega}/K$ emphasizes that the $H_{\varepsilon\Omega}(s)$ zero is unstable in Region 3. The system having a non-minimum phase behaviour, then the power controller design must be chosen accordingly. Table 2 presents the values of each term appearing in the transfer function $H_{\varepsilon\Omega}(s)$, for each of the two operating points op_1 and op_2 defined by (9).

In conclusion, as the system passes from minimum-phase behaviour in Region 2 to non-minimum-phase behaviour in Region 3, the adopted control design methods will be different in the two regions. Thus, the root locus method will be used for Region 2 and the general version of the maximum flat method will be employed in Region 3, as detailed next.

3.2 Power Controller Design in Region 2 (Partial Load)

Table 2 allows us determining the plant $H_{\varepsilon\Omega}(s)$ around the operating point denoted by op_1 as:

$$H_{\varepsilon\Omega}(s) = \frac{-98.7983(s + 1.0695)}{s^2 + 4s + 11.11} \tag{18}$$

Taking account of the plant transfer function form (18) – with one zero and two complex-conjugated poles – one can employ the usual root locus method in order to get the parameters of a PI power controller (Munteanu *et al.* (2008)). The implementation of this method in MATLAB® (function *rltool*) leads to obtaining the following power optimization controller:

$$H_{PIP}(s) = k_{p2} \cdot \frac{T_{i2}s + 1}{T_{i2}s} = -0.016 \cdot \frac{1 + 0.086s}{0.086s} \tag{19}$$

Using the controller (19) for operating points other than the ones for which it has been computed will obviously lead to altering the dynamic performance. One can however note that the slopes of the wind torque and electromagnetic torque characteristics do not vary significantly when the operating point moves along the ORC. Therefore, the PI power control performance is practically not affected. Indeed, results provided by MATLAB function *rltool* show that the phase margin does not become less than 60^0 for any operating point on the ORC.

3.3 Power Controller Design in Region 3 (Full Load)

Knowing that the plant exhibits non-minimum phase behaviour in Region 3, the power controller may be computed using the general version of the modulus optimum criterion (*maximum flat method*). With the PI power controller

$$H_{PIP}(s) = k_{p3} \frac{T_{i3}s + 1}{T_{i3}s}, \tag{20}$$

the closed-loop transfer function may be written as:

$$H_{0P}(s) = \frac{a_2 s^2 + a_1 s + a_0}{b_3 s^3 + b_2 s^2 + b_1 s + b_0}, \tag{21}$$

where the coefficients have the expressions:

$$\begin{cases} a_2 = k_{p3} T_{i3} k_p T k_{em} \overline{\Omega} \\ a_1 = k_{p3} \left[T_{i3} \left(\overline{\Omega} - K \overline{T_{em}} \right) + \overline{\Omega} T \right] k_{em} k_p \\ a_0 = k_{p3} k_{em} k_p \left(\overline{\Omega} - K \overline{T_{em}} \right) \\ b_3 = T \cdot T_i T_{i3} \\ b_2 = T_{i3} \left[T_i \left(1 - k_p k_{em} K \right) + k_{p3} \overline{\Omega} T k_{em} k_p \right] \\ b_1 = k_{em} k_p \left[k_{p3} \left(\overline{\Omega} T + T_{i3} \left(\overline{\Omega} - K \overline{T_{em}} \right) \right) - K T_{i3} \right] \\ b_0 = k_{em} k_p k_{p3} \left(\overline{\Omega} - K \overline{T_{em}} \right) \end{cases} \quad (22)$$

with notation $\overline{\bullet}$ corresponding to the operating point op_2 from (9). The closed-loop squared gain, $\left| H_{0P}(j\omega) \right|^2$, is:

$$\left| H_{0P}(j\omega) \right|^2 = \frac{a_2^2 \omega^4 + \left(a_1^2 - 2a_0 a_2 \right) \omega^2 + a_0^2}{b_3^2 \omega^6 + \left(b_2^2 - 2b_1 b_3 \right) \omega^4 + \left(b_1^2 - 2b_0 b_2 \right) \omega^2 + b_0^2} \quad (23)$$

The general version of the maximum flat method requires that the closed-loop squared gain to meet the form (Ceangă, E. *et al.* (2001)):

$$\left| H_{0P}(j\omega) \right|^2 = \frac{A(\omega^2)}{b_3^2 \omega^6 + A(\omega^2)},$$

hence the following equalities must hold:

$$\begin{cases} a_2^2 = b_2^2 - 2b_1 b_3 \\ a_1^2 - 2a_0 a_2 = b_1^2 - 2b_0 b_2 \end{cases} \quad (24)$$

Computation combining (22) and (24) with parameter values corresponding to op_2 given by (9) finally leads to solving the equation system:

$$\begin{cases} 0.04 \cdot T_{i3} - 58.48 \cdot k_{p3} \cdot T_{i3} + 3.6 \cdot k_{p3} = 0 \\ 8.9 \cdot T_{i3} - 393.02 \cdot k_{p3} + 1043.2 \cdot k_{p3} T_{i3} = 0 \end{cases},$$

whose solution is $k_{p3} = 0.0024$ and $T_{i3} = 0.084$.

Concerning the performance of the power limitation controller when the operating moves along the whole Region 3, one can make similar remarks like in the case of the power optimization controller. Indeed, the torque curves from Fig. 2 suggest that the slopes responsible for the dynamic behaviour do not change very much along Region 3 (*i.e.*, when the wind speed is larger than 10 m/s); therefore, one cannot expect but slight alteration of the power limitation controller performance when the operating point changes.

4. EXPERIMENTAL RESULTS

The proposed power control structure has been experimentally validated using a test rig with the structure presented in Fig. 7. The wind turbine has been replaced by a electromechanical wind turbine simulator. This provides a "turbine shaft" where the steady-state and dynamic characteristics of a given turbine can be replicated (Munteanu *et al.* (2010), Li *et al.* (2006), Abdelkarim *et al.* (2012)). Some parameters of the test rig are given in the Appendix.

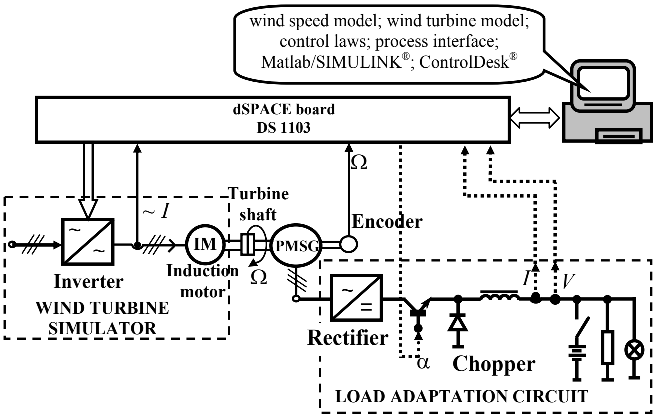

Fig. 7. The wind turbine simulator diagram.

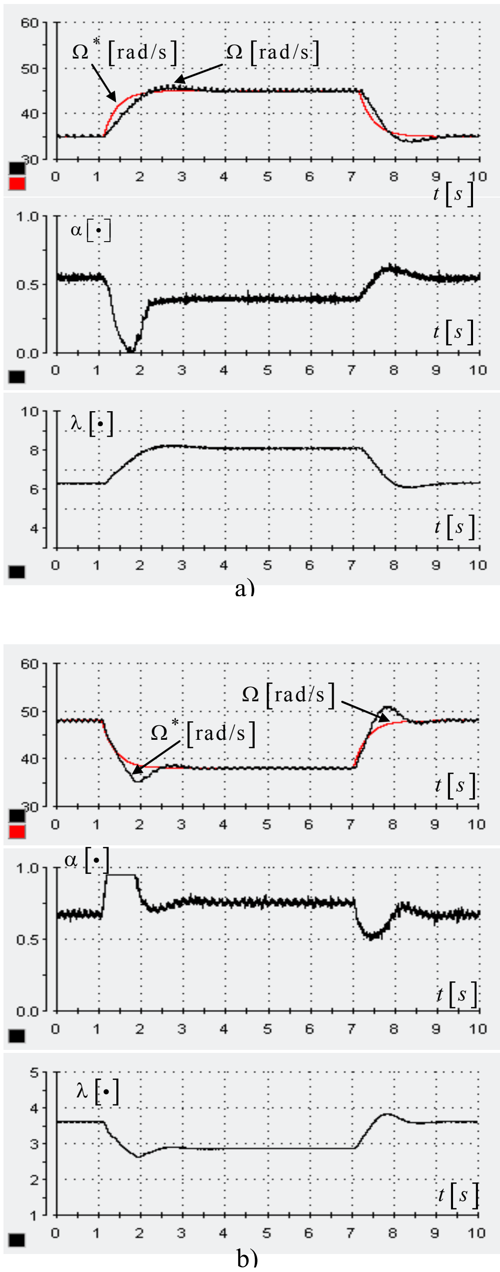

Fig. 8. Closed-loop speed behavior in: a) partial-load regime $(v = 5 \text{ m/s})$; b) full-load regime $(v = 12 \text{ m/s})$.

The first experimental test is performed to show the rotational speed closed-loop dynamic performance in both partial-load and full-load regimes (at constant wind speed). The rotational speed reference, Ω^*, is applied through a filter, in order to avoid excessive control effort.

Fig. 8a presents the results obtained when system is running near ORC (Region 2) at a wind speed of 5 m/s, the rotational speed varying from 35 rad/s to 45 rad/s. Fig. 8b shows the system response when operating in Region 3, at a wind speed of 12 m/s, when the rotational speed reference changes from 48 rad/s to 38 rad/s. The results show different (but stable) dynamic behaviours for the two considered cases. Note that the system operation in full load supposes the severe reduction of the tip speed ratio (by active speed stall).

Fig. 9 shows the power-controlled WECS response in both partial-load and full-load regimes. In order to evaluate the power loop performances, wind speed steps have been applied.

A wind speed step from 5.5 m/s to 6.5 m/s (see the detail of the wind speed variation in Fig. 9a) determines a relatively slow power evolution in Region 2a. The rotational speed evolves such as the operating point regains the ORC in steady-state (in about 5 seconds); this is also shown by the tip speed ratio evolution towards its optimal value ($\lambda_{opt} = 7$). Concerning the rotational speed, the detail from the left side of the graph shows that the rotational speed tracks the reference Ω^* after an initial fast deviation. This initial deviation (of about 5%) is the result of the direct wind speed action over the rotational speed (see the plant structure in Fig. 6a). This effect is further mitigated by the rotational speed loop action which determines the rotational speed tracking. Practically, there are two superposed effects: the disturbance direct effect and the rotational speed tracking effect. The second detail (right side of the rotational speed evolution in Fig. 9a) shows that the steady-state value is less than the limitation one (in this case, 50 rad/s).

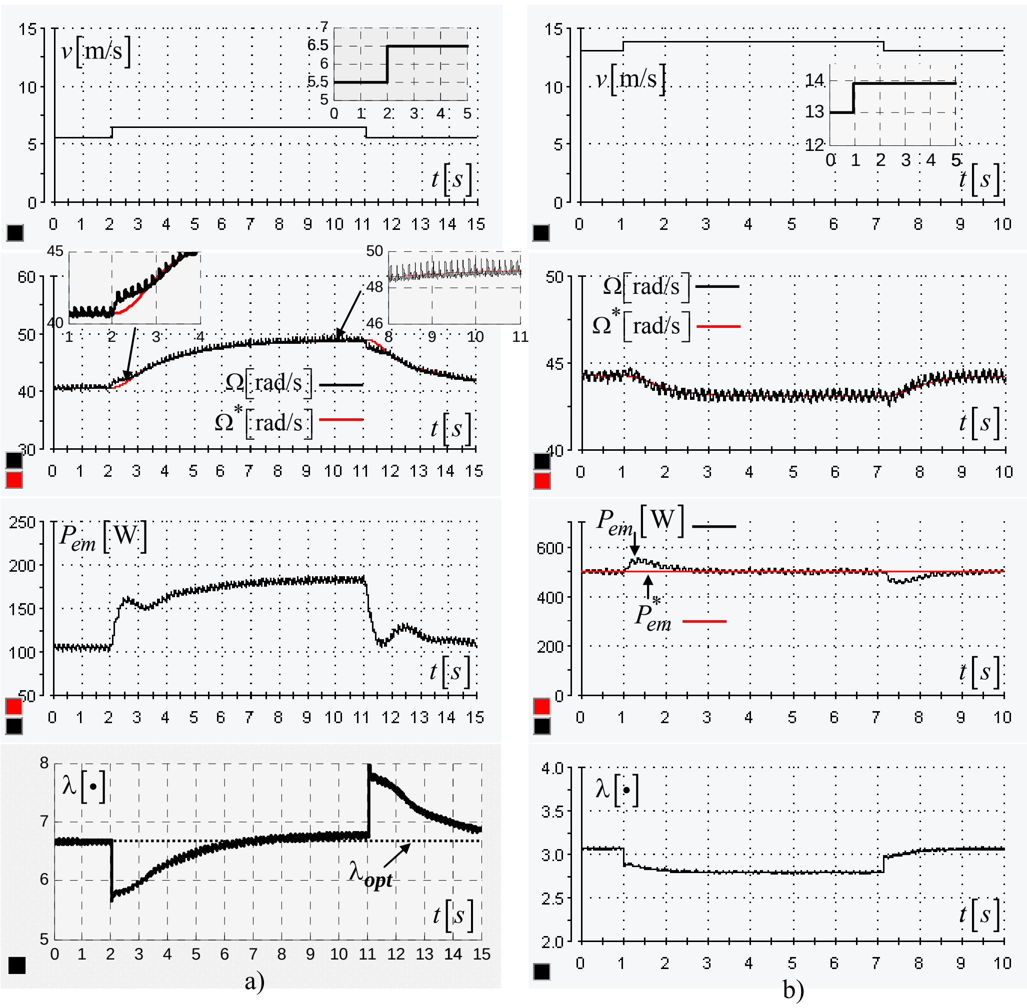

Fig. 9. Power loop responses for different wind speed steps: a) in Region 2a; b) in Region 3

This quite slow dynamic response is suitable in Region 2a where the wind turbulence is not so important (Nichita. *et al.* 2002). Fig. 9b allows the power control performance assessment when operating in Region 3.

A wind speed step variation (from 13 m/s to 14 m/s) induces a reduction in the rotational speed in order to maintain the prescribed power value ($P_{lim} = 500$ W). The maximum power deviation is 10% and the disturbance effect is zeroed in about one second.

As the wind speed increases, the wind turbine is driven in deeper stall as the tip speed ratio, λ, decreasing evolution suggests. In Fig. 10 one can analyze the power closed-loop responses when the operating point moves between Regions 2a and 2b (Fig. 10a) and from Region 2b to 3 and backwards (Fig. 10b).

A wind step from 6 m/s to 8 m/s ensures the operating point transition from Region 2a to Region 2b. The rotational speed has a transition from a lower value corresponding to the power optimization zone to the limitation value (50 rad/s) corresponding to the operating Region 2b. The direct effect of the disturbance (wind speed variation) – already revealed in Fig. 9a – is even clearer here.

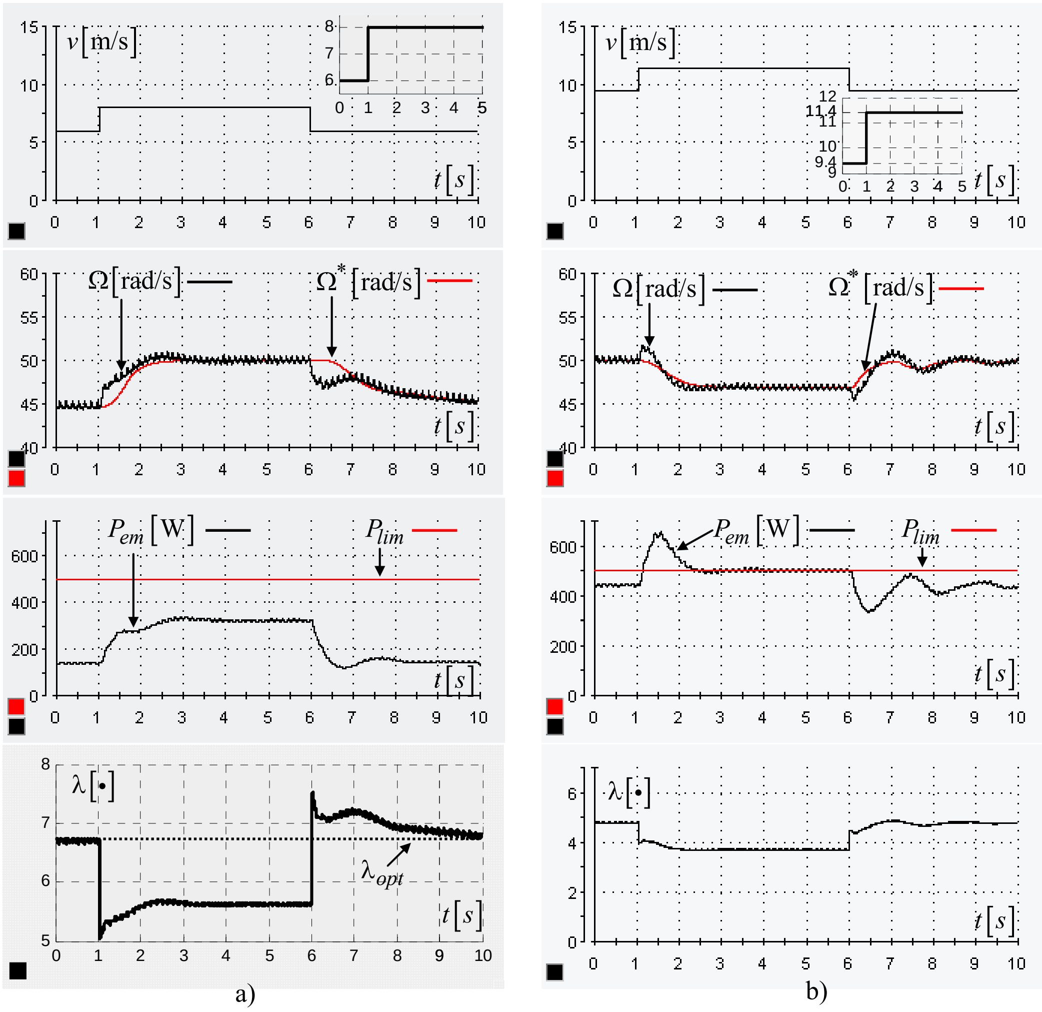

Fig. 10. WECS response to wind speed steps: a) from Region 2a to Region 2b and backwards; b) from Region 2b to Region 3 and backwards.

Regarding the tip speed evolution, one can note that it evolves from its optimal value $\lambda_{opt} = 7$ towards a lower value (due to a limitation in rotational speed and to a larger value of wind speed). As the system exits from rotational speed limitation, the rotational speed maximal deviation is about 5%.

When the wind speed evolves from 9.4 m/s to 11.4 m/s (Fig. 10b) the operating point passes from Region 2b to Region 3, the dynamic response lasting for about 2.5 s. The wind speed variation determines an electromagnetic power variation such that the power reference to be switched from $K_{wt}\Omega^3$ to P_{lim}. This switching occurs when $P_{em} = 0.8 \cdot P_{lim}$. When passing in Region 3, the power is limited by reducing the rotational speed value. Consequently, the tip speed ratio decreases, the WECS begins entering in stall. The overpower dynamic regime lasts for about one second with a maximum deviation from the setpoint of about 22%. As the wind speed decreases, the electromagnetic power decreases also below $0.8 \cdot P_{lim}$, and the system enters in Region 2b, by limiting the rotational power to 50 rad/s. One can note that, irrespective of how a transition between two regions is made, the direct effect of the wind speed variation over the rotational speed behaviour (see Fig. 6a) is always present, even if is further alleviated by the control loop action.

The maximum power deviation with respect to its reference occurs at the transition from Region 2b to Region 3 in presence of highly variable wind speed. The maximum rotational speed deviation occurs when the system passes from Region 2b to Region 2a (the WECS exits the rotational speed limitation zone as the wind speed decreases rapidly). The rotational speed slightly overpasses the imposed limit of

$\Omega_{lim} = 50$ rad/s in Region 2b, but these overshoots are practically insignificant.

5. CONCLUSIONS

This paper concerns the power control of the fixed-pitch small-power wind turbines with PMSG, where the power limitation is performed by an active speed stall control. As the plant models essentially differ in partial-load and in full-load regime, different methods have employed in order to design the respective power controllers design. However, the rotational speed is controlled by a unique controller. Its parameters are chosen in order to ensure satisfactory performances, when the plant's characteristic varies significantly over the entire operating range. Concerning the power loop, the transitions between Region 2b and Region 3 are accompanied not only by changes of the plant model, but also by the control input phase reversal.

As the plant dynamic in power maximization is a minimum-phase second-order one, the root locus method has consequently been chosen for the associated power controller design. In power limitation region the WECS exhibits a non-minimum-phase behaviour; therefore, the associated power controller results according to the general version of the maximum flat design method.

The performed experiments highlight the satisfactory dynamic system performances in each operating regime. For both power and rotational speed controllers, experimental results validate, with tolerable dynamic deviations, the analytic parameters computation.

REFERENCES

Abdelkarim, M., Lotfi, K., and Abderrazak, O. (2012) “Voltage control of a variable speed wind turbine connected to an isolated load: Experimental study,“ Energy Conversion and Management, vol. 59, pp. 19–26

Åström, K.J., and Hägglund, T. (1995) *PID controllers: theory, design and tuning*, 2nd edn. Instrument Society of America

Bang, D., Polinder, H., Shrestha, G., Ferreira, J.A., and van Rooij, R.P.J.O.M (2007) “New active speed stall control compared to pitch control for direct-drive wind turbines”, EWEC (European Wind Energy Conference & Exhibition, Milan, Italy, May 7-10

Bianchi, F., De Battista, H., and Mantz, R.J. (2006). *Wind turbine control systems – Principles, modelling and gain scheduling design*. Springer-Verlag, London, 2006.

Burton, T., Sharpe, D., Jenkins, N., and Bossanyi, E. (2001). *Wind energy handbook*. John Wiley & Sons, New-York

Ceangă, E., Protin, L., Nichita, C., and Cutululis, N.-A. (2001) *Theory of control systems* (in French: Théorie de la commande des systèmes). Technical Publishing House, Bucharest, Romania

Hoffmann, R. (2002) *A comparison of control concepts for wind turbines in terms of energy capture*, PhD Thesis, Darmstadt University

Li, H., Steurer, M., Shi, K.L., Woodruff, S., and Zhang, D. (2006) “Development of a Unified Design, Test, and Research Platform for Wind Energy Systems Based on Hardware-in-the-Loop Real-Time Simulation,” IEEE Transactions on Industrial Electronics, vol. 53, no. 4, pp. 1144-1151

Munteanu, I., Bratcu, A.I., Cutululis, N.-A., and Ceangă, E. (2008). *Optimal Control of Wind Energy Systems – Towards a Global Approach*. Springer-Verlag London

Munteanu, I., Bratcu, A.I., Bacha, S., Roye, D., and Guiraud, J. (2010) “Hardware-in-the-Loop-based Simulator for a Class of Variable-speed Wind Energy Conversion Systems: Design and Performance Assessment,” IEEE Transactions on Energy Conversion, vol. 25, no. 2, pp. 564-576

Nichita, C., Luca, D., Dakyo, B., and Ceangă, E, (2002) “Large band simulation of the wind speed for real time wind turbine simulators,” IEEE Transactions on Energy Conversion, vol. 17, no. 4, pp. 523-529

Polinder, H., Bang, D., van Rooij, R.P.J.O.M., McDonald, A.S, and Mueller, M.A. (2007) “10 MW Wind turbine direct-drive generator design with pitch or active speed stall control”, IEEE Int. Electric Machines and Drives Conf., Antalya, Turkey, May 3-5

Scarlat, A., Munteanu, I., Bratcu, A.I., and Ceangă, E. (2010) “Use of a configurable torque-speed dependence for power maximization of squirrel-cage-induction-generator-based wind energy conversion system” AGIR “Gheorghe Asachi” Technical University of Iaşi, LVI (LX), Fasc. 4, pp.41-60

Şerban, I., and Marinescu, C. (2012) “A sensorless control method for variable-speed small wind turbines” Renewable Energy, vol. 43, pp. 256–266

Vihriälä, H. (2002). *Control of Variable Speed Wind Turbines*. PhD Thesis, Tampere University of Technology

Vlad, C., Munteanu, I., Bratcu, A.I., and Ceangă, E. (2009) “Anticipative Control of Low-Power Wind Energy Conversion Systems for Optimal Power Regime,” Control Engineering and Applied Informatics, vol. 11, no. 4, pp. 26-35

APPENDIX

Wind turbine data

Optimal tip speed ratio $\lambda_{opt} = 7$, maximum power coefficient $C_{p\max} = 0.476$, blade length $R = 0.9$ m, total inertia $J = 0.2\ \mathrm{kg \cdot m^2}$

Torque coefficient parameters:

$a_0 = 0.0061$, $a_1 = -0.0013$, $a_2 = 0.0081$, $a_3 = -9.7477 \cdot 10^{-4}$, $a_4 = -6.5416 \cdot 10^{-5}$, $a_5 = 1.3027 \cdot 10^{-5}$, $a_6 = -4.54 \cdot 10^{-7}$

Energy conversion chain data

PMSG 48 V, 5 pole pairs, *L*=10 mH / 25 A, Chopper with IGBT IRG4PC40FD, PWM 20 kHz, DC-link voltage 24 V
Current controller parameters: $k_i = 100$, $k_p = 0.03$